Pis'ma v ZhETF, vol. 94, iss. 2, pp. 157 – 165

ПО ИТОГАМ ПРОЕКТОВ
РОССИЙСКОГО ФОНДА ФУНДАМЕНТАЛЬНЫХ ИССЛЕДОВАНИЙ
Проект РФФИ # 08-02-00005а

Electron loss of heavy many-electron ions in relativistic collisions with neutral atoms

I. Yu. Tolstikhina, V. P. Shevelko[1)]

P.N. Lebedev Physical Institute, 119991 Moscow, Russia

Submitted 10 May 2011

Electron-loss processes arising in collisions of heavy many-electron ions (like U^{28+}) with neutral atoms (H, N, Ar) are considered over a wide energy range including relativistic energies. Various computer codes (LOSS, LOSS-R, HERION and RICODE), created for calculation of the electron-loss cross sections, and their capability are described. Recommended data on the electron-loss cross sections of U^{28+} ions colliding with H, N, Ar targets and predicted lifetimes of U^{28+} ion beams in accelerator are given. Calculated electron-loss cross sections are compared with available experimental data and other calculations.

1. Charge-changing processes. Electron loss (EL), also called electron stripping or ionization of the projectile, occurs in collisions of ions with atoms or molecules

$$X^{q+} + A \to X^{(q+m)+} + \Sigma A + me^-, \quad m \geq 1, \qquad (1)$$

where X^{q+} denotes the incident projectile ion with a charge q and A represents the target atom (or molecule), respectively. ΣA indicates that the outgoing target atom A can be excited or even ionized.

In general, for many-electron projectiles the reaction (1) involves multiple-electron losses ($m > 1$), a contribution of which to the total electron-loss cross sections can be more than 50%. With energy increasing multiple-electron losses become small and single-electron loss processes ($m = 1$) prevail, especially, in the relativistic energy range.

Electron loss together with electron capture (EC)

$$X^{q+} + A \to X^{(q-k)+} + A^{k+}, \quad k \geq 1, \qquad (2)$$

constitute two main charge-changing processes playing a critical role in many fields of atomic, accelerator and plasma physics, such as heavy-ion fusion (HIF) program [1], particle tumor therapy [2], heavy-ion probe beam (HIPB) diagnostics in plasma devices [3] as well as the design of synchrotrons and beam transport structures. In particular, the International FAIR project (Facility for Antiproton and Ion Research) started recently at GSI, Darmstadt [4], where heavy many-electron ions (like U^{28+}) are planned to be accelerated up to relativistic energies of a few tens of GeV/u, requires benchmarks for EL cross sections as EL-processes can dominate among other beam-loss processes. Single and multiple EL-processes are a subject of intensive experimental studies at GSI (Germany), ITEP and JINR (Russia), A&M Texas cyclotron (USA) and LIER (CERN).

A typical example of the cross sections for two competing charge-changing processes, loss and capture, is given in Fig. 1 for U^{42+} ions (50 electrons) colliding with Ar atoms as a function of collision energy. In general, cross sections for both EL- and EC-processes are rather large. At low energies, EC prevails and is characterized by a quasi-constant behavior whereas at high energies, EL is the main charge-changing process, which also has a quasi-constant cross section in the relativistic energy range. The position of the crossing point of both cross sections ($E \sim 7$ MeV/u) strongly depends on the atomic structure of both colliding particles.

At present, experimental and theoretical data on relativistic ion-atom collisions are available mainly for a few-electron ions (H- and He-like) whereas for many-electron projectiles these data are practically absent. However, requirements for vacuum conditions and ion-beam lifetimes in accelerators are directly related with accurate knowledge of electron loss cross sections of heavy ions colliding with residual-gas atoms and molecules.

[1)] e-mail: shev@sci.lebedev.ru

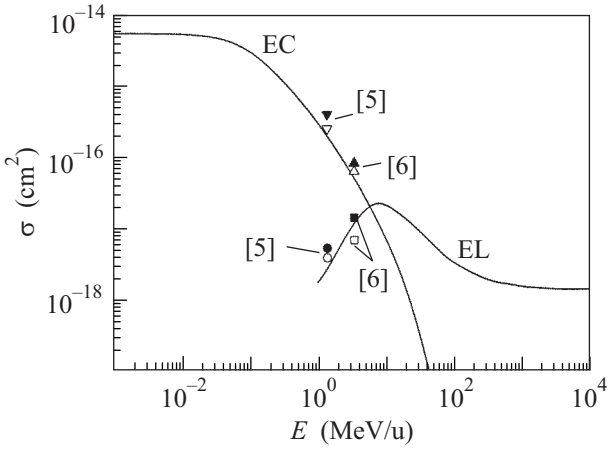

Fig. 1. Charge-changing cross sections in U^{42+} + Ar collisions as a function of collision energy. Experimental data on single-electron capture and loss cross sections (open symbols) are given to show their contribution to the total cross sections (solid symbols). Solid curves: EC – calculations by the CAPTURE code, and EL – by DEPOSIT and RICODE codes (see [7] for description of the codes)

Relativistic ion-atom collisions involving H- and He-like like highly charged ions are considered in various books [8, 9] and review articles [10, 11]. Since the relativistic wave functions for H-like ions are known, the corresponding calculations can be used to check the applicability of the first-order perturbation theory and the influence of the so-called *magnetic* interactions arising between colliding particles at relativistic energies.

The aim of this work is to present a recent progress in theoretical calculations of electron-loss cross sections for heavy many-electron ions colliding with neutral atoms over a wide energy range including relativistic energies. A brief description of methods and recently created computer codes (LOSS, LOSS-R, HERION and RICODE) for calculations of electron-loss cross sections is given. Recommended data on EL cross sections for U^{28+} ions colliding with H, N and Ar targets (main residual-gas components) are presented.

Atomic units are used: $m = e = \hbar = 1$.

2. Non-relativistic approximation. The LOSS-code. Over the last ten years, electron loss processes in the non-relativistic energy range, $1\,\mathrm{MeV/u} < E < 100\,\mathrm{MeV/u}$, were investigated experimentally and theoretically in more details. At present, two main different approaches are used in this range: a classical approximation (classical trajectory Monte Carlo (CTMC) method [12] and energy-deposition model [13]) and a quantum-mechanical non-relativistic Born approximation [14]. Classical approximation approaches are used to describe single-, multiple-electron loss and total loss cross sections, and the Born approximation for a single-electron loss cross sections. It is important to note that in the case of many-electron projectile ions, a contribution of multiple-electron losses to the total loss cross sections can be very large and reach up to more than 50%, therefore, at low and intermediate energies, $1\,\mathrm{MeV/u} < E < 10\,\mathrm{MeV/u}$, the classical models give more accurate results compared to the Born approximation which is applied for single-electron loss calculations. But at higher energies, $E > 10\,\mathrm{MeV/u}$, the Born approximation is preferable because the results in the classical approximation overestimate experimental data. As a result, two different approximations give different asymptotic behavior for the total loss cross sections: $\sigma_{\mathrm{tot}} \sim E^{-1}$ in the Born approximation and $\sigma_{\mathrm{tot}} \sim E^{-a}$ in the classical approximation where the constant a varies approximately in the limits $0.3 \le a \le 0.9$ depending on the target atomic number (e.g., $a = 0.3$ for Xe and $a = 0.9$ for H).

In the non-relativistic plane-wave Born approximation (PWBA), the single-electron loss cross section in the momentum-transfer Q-representation is given by [14]:

$$\sigma(v) = \frac{8\pi}{v^2} \sum_{nl} N_{nl} \sum_{\lambda} \int_0^{\infty} d\varepsilon \int_{Q_0}^{\infty} \frac{\mathrm{d}Q}{Q^3} Z_T^2(Q) F_P^2(Q, nl, \varepsilon, \lambda), \tag{3}$$

$$|F_P(Q, nl, \varepsilon, \lambda)|^2 = \left| \langle \varepsilon\lambda | \exp(i\mathbf{Qr}) | nl \rangle \right|^2, \; Q_0 = \frac{I_{nl} + \varepsilon}{v}, \tag{4}$$

$$|Z_T(Q)|^2 = \left[Z - \sum_{j=1}^{N} \langle j | \exp(i\mathbf{Qr}) | j \rangle \right]^2 + \left[N - \sum_{j=1}^{N} | \langle \exp(i\mathbf{Qr}) | j \rangle |^2 \right]. \tag{5}$$

Here v denotes a relative velocity, $F_P(Q)$ – the projectile form-factor, $Z_T(Q)$ – the effective charge of the target atom, Z and N – the target nuclear charge and total number of electrons, ε and λ – the energy and orbital momentum of the ejected projectile electron to be ejected, I_{nl} and N_{nl} – the binding energy and number of equivalent electrons of the projectile shell nl. For neutral atoms one has $Z = N$ and for protons $Z_T(Q) = 1$. Q_0 in eq. (4) is the minimal momentum which can transferred to the projectile from the target after collision. $|nl\rangle$ and $|\varepsilon\lambda\rangle$ denote the wave functions of the projectile electron in the initial and final states and $|j\rangle$ denotes a wave function of outermost and inner-shell target electrons.

Equations (3)–(5) were realized in the LOSS computer code [7] where the wave functions of the bound

$|nl\rangle$ and and continuum $|\varepsilon\lambda\rangle$ states of the projectile active electron are found by numerical solution of the non-relativistic Schrodinger equation, and those for the target $|j\rangle$ are calculated with the nodeless Slater functions. The atomic structure of the target is taken into account through the dependence of the effective charge $Z_T(Q)$, eq. (5) on the momentum trasfer Q.

The use of the non-relativistic wave functions for many-electron heavy projectiles is justified because the main contribution to the loss cross sections at high collision energies is given by the loss of outermost projectile electrons which can be treated as non-relativistic particles.

In the LOSS-code, the calculated cross sections decrease with the projectile energy increasing in accordance with the Born approximation:

$$E \to \infty, \quad v \to \infty, \quad \sigma \to \frac{\ln v}{v}. \tag{6}$$

We note, that in the case of molecular targets, the Bragg's additive rule is usually used, i.e., the interaction with a molecule is presented as a sum of interactions with individual atoms composing the molecule, e.g., for CO_2 target one has $\sigma(CO_2) = \sigma(C) + 2\sigma(O)$. A typical example of EL-cross sections for $U^{28+} + N_2$ collisions is shown in Fig. 2 where experimental data are compared with LOSS-code and CTMC calculations.

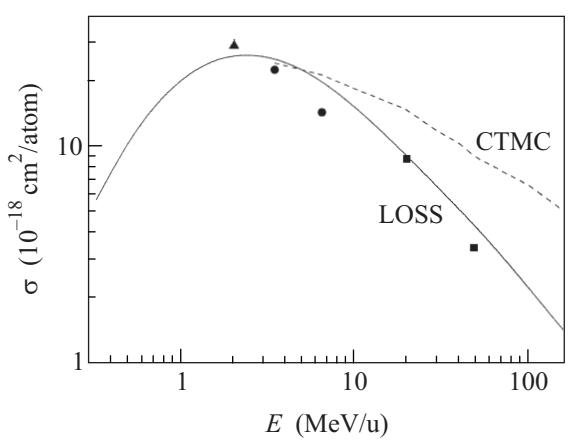

Fig. 2. Electron-loss cross sections in $U^{28+} + N_2$ collisions as a function of collision energy. Experiment: ▲ [15], ● [16], ■ [17]. Solid curve – LOSS-code, dashed curve – CTMC calculations [16]

3. Relativistic version of the LOSS-code: the LOSS-R code. Because the non-relativistic LOSS-code can not be used at relativistic energies $E > 100$ MeV/u, it was an attempt to extend the LOSS-code to the relativistic energy range and to create the LOSS-R-code (Relativistic LOSS). The LOSS-R code uses the same equations (3)–(5) and non-relativistic wave functions but with the following changes [18]:

$$v \to \beta c, \quad Q_0 \to \frac{I_{nl} + \varepsilon}{\gamma v}, \tag{7}$$

where β and γ denote the relativistic factors, and c the speed of light. At relativistic energies, the LOSS-R-code provides the following asymptotic behavior (cf eq. (4)):

$$E \to \infty, \quad v \to c, \quad \sigma \to \ln\gamma. \tag{8}$$

Obviously, at non-relativistic energies, the results obtained by the LOSS-R code coincide with those obtained by the LOSS code.

The main difference between two codes is that in the LOSS-R-code the minimum momentum transfer Q_0 is γ times smaller than Q_0 in the LOSS-code. This *ad hoc* approximation was motivated by the fact that the expression similar to Q_0 in eq. (7) was obtained by Bethe [19] from estimation of the energy transferred to an atom by incident heavy particle at relativistic energies (see also [20]). However, despite of this rough approximation, the LOSS-R-code gives quite good overall results for relativistic electron-loss cross sections compared to experimental data and more sophisticated calculations (see section 5 RICODE).

Fig. 3 shows a behavior of ionization cross sections of K-shell electrons of Zr ($Z = 40$), Tb ($Z = 65$) and U ($Z = 92$) neutral atoms in collisions with protons as a

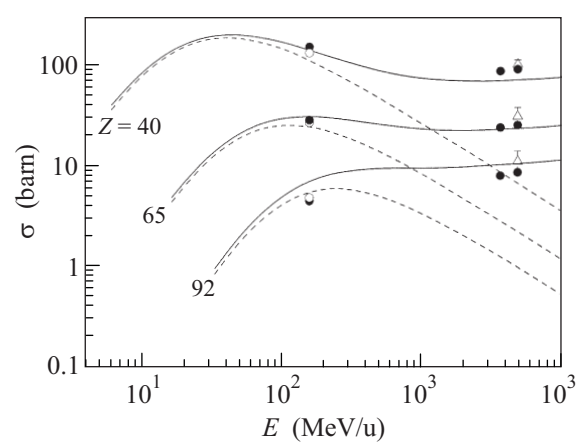

Fig. 3. Proton K-shell ionization cross sections of atoms with atomic numbers $Z = 40$, 65 and 92 as a function of the proton energy: triangles – experimental data at 4.88 GeV [21]; open and solid circles – non-relativistic and relativistic calculations of Davidovic et al [22] at proton energies of $E = 0.16$, 3.672 and 4.88 GeV, respectively, solid and dashed curves – relativistic and non-relativistic calculations by the LOSS-R and LOSS-codes, respectively. From [18]

function of proton energy. As is seen, the non-relativistic cross sections (LOSS-code) decrease with energy increasing meanwhile the relativistic cross sections show a slightly increasing behavior at energies $E > 400\,\mathrm{MeV/u}$ and at $E = 10\,\mathrm{GeV/u}$ the difference between two approximations is about one order of magnitude. The agreement between experimental data, relativistic calculations by Davidovic and results by the LOSS-R-code is within 30%.

Another example of relativistic ion-atom collisions is shown in Fig. 4 where experimental and theoretical data

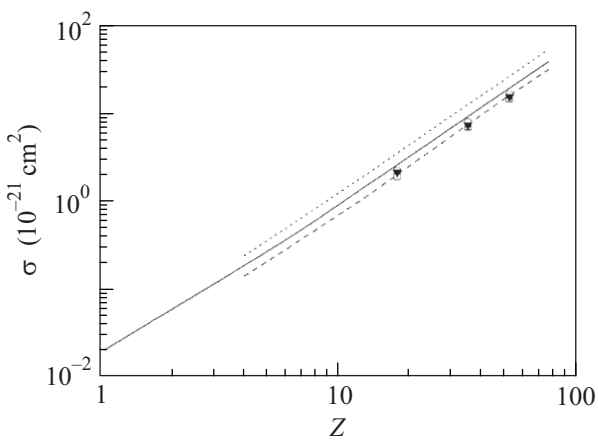

Fig. 4. Electron-loss cross sections of H-like $Pb^{81+}(1s)$ ions colliding with gaseous atoms at ultra-relativistic energy of 158 GeV/u ($\gamma = 170$) as a function of the target atomic number Z. Experiment for Ar, Kr and Xe atoms: □ [24]. Theory: dotted curve – plane-wave Born approximation [25], dashed curve – relativistic model [26], ○ – sudden approximation [27], ▼ – relativistic calculations [11], and solid curve – the LOSS-R results [18]

on electron-loss cross sections of H-like lead ions colliding with gaseous atoms are shown at ultra-relativistic energy $E = 158\,\mathrm{GeV/u}$ ($\gamma = 170$). As in Fig. 3, experimental and theoretical results agree within 20–30%. In the case of solid targets, calculations of the EL cross sections are much more complicated because in solid targets one has to account for the so-called *target-density effects* (see [11], [23] for details).

4. Dipole and impulse approximations. HERION-code. Electron loss processes at relativistic energies was also considered in the impact parameter b-representation when the whole range of impact parameters can be divided into two ranges: large and small b-values. Then at large b, the *dipole* interaction between colliding particles plays the main role, interaction between projectile active electron and the target atom is small and transition occurs with a small energy transfer that makes it possible to apply the perturbation theory. At small impact parameters an *impulse* approximation can be used because a transferred energy is large and interaction area is small. As a result, the EL cross section can be presented as a sum of two terms: dipole and non-dipole onces

$$\sigma(v) = \sigma_{\mathrm{dip}}(v) + \sigma_{\mathrm{non-dip}}(v). \tag{9}$$

The dipole term $\sigma_{\mathrm{dip}}(v)$ can be calculated via the photoionization cross section $\sigma_{\mathrm{ph}}(\omega)$ and the so-called the number of equivalent photos $n(\omega)$ provided the effective charge of the atomic target Z_{eff} does not depend on the impact parameter b [10]:

$$\sigma_{\mathrm{dip}}(nl, v) = \int\limits_{\omega_{\min}}^{\infty} n(\omega)\sigma(nl,\omega)\frac{d\omega}{\omega}, \tag{10}$$

$$n(\omega) = \frac{2Z_{\mathrm{eff}}^2}{\pi(\beta c)^2}\times$$

$$\times\left\{xK_0(x)K_1(x) - \frac{1}{2}(\beta x)^2[K_1^2(x) - K_0^2(x)]\right\}, \tag{11}$$

$$x = \frac{\omega b_{\min}}{\gamma\beta c}, \quad b_{\min} = \frac{n}{(2I_{nl})^{1/2}}, \tag{12}$$

where I_{nl} denotes the binding energy of the projectile electronic shell nl from which electron is removed, $\sigma_{\mathrm{ph}}(nl,\omega)$ – the corresponding photoionization cross section, β and γ – relativistic factors, and $K_m(x)$ – the MacDonald functions.

The non-dipole part can be calculated in the impulse approximation and has the form [29]:

$$\sigma_{\mathrm{non-dip}}(nl, v) = \frac{2\pi N_{nl}}{I_{nl}}\left(\frac{Z_{\mathrm{eff}}\alpha}{\beta}\right)^2, \tag{13}$$

where N_{nl} is the number of equivalent electrons in the nl shell.

Equations (9)–(13) were realized in the HERION computer code (High-Energy Relativistic IONization) which applies the *relativistic* Dirac–Fock wave functions for calculation of the photoionization cross sections (see [29] for description of the code). The code can be applied at collision energies $E > 100\,\mathrm{MeV/u}$ but it does not account for the magnetic interactions (see section 5).

Calculations of the relativistic electron-loss cross sections of uranium ions by proton impact ($Z_{\mathrm{eff}} = 1$) performed by HERION- and LOSS-R-codes showed [29] that the results by HERION code can be a factor of 2 larger or smaller than those obtained by the LOSS-R-code. Such behavior can be explained by the use of different wave functions in the codes (relativistic Dirac–Fock in the HERION and non-relativistic Schrödinger

wave functions in the LOSS-R-code), and some other reasons related with calculation of the photoionization cross sections (see [29] for details). Calculations by the HERION-code showed that the dipole part of the electron-loss cross sections involves about 60–70% of the total cross section while the relativistic non-dipole part has a weak dependence on collision energy, and, therefore, the dipole part has almost the same shape as the total cross section. These features are shown in Fig. 5 for relativistic ionization cross sections of U^{28+} ions by proton impact.

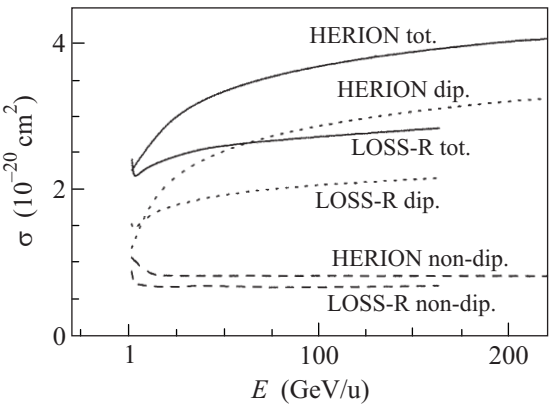

Fig. 5. Relativistic dipole, non-dipole and total ionization cross sections of U^{28+} ions induced by proton impact: HERION dip. – the HERION-results, dipole approximation, eqs. (9)–(12), HERION non-dip. – non-dipole part of the cross section, impulse approximation, eq. (13), LOSS-R dip. – the LOSS-R-results including only dipole transitions of the projectile electron into continuum, LOSS-R non-dip. – the LOSS-R results including only non-dipole transitions into continuum, HERION tot. and LOSS-R tot. – the sum of dipole and non-dipole parts, respectively. From [29]

5. Relativistic Born approximation. The RICODE computer program. A more correct and consistent way to improve the LOSS-R-code for relativistic ionization of the projectile was to include the relativistic (magnetic) part of the interaction between colliding particles in the ionization matrix element which in general has the form [8]:

$$M_{if} = \langle f|(1-\beta\alpha_Z)e^{i\mathbf{Qr}}|i\rangle\,, \qquad (14)$$

where $\beta = v/c$ denotes the relativistic factor, c – the speed of light, α_z – the z – component of the Dirac matrix α, and Q the momentum transfer; $|i\rangle$ and $|f\rangle$ are the total wave functions of the system in the initial and final states, respectively.

The first term in eq. (14) is related to a contribution of a scalar potential of the field created by a neutral target and corresponds to the "usual" non-relativistic Born form-factor, eqs. (3)–(5). The second term, often called "magnetic interaction", describes a contribution of a vector potential of the target-atom field. Calculation of the matrix elements (14) with the second term is a very complicated problem which was realized mainly for ionization of H- and He-like ions for ionization from the bound states with the principal quantum numbers $n = 1-6$ (see [8, 28, 30]). In the work [31], using the Coulomb gauge for the atomic field of the target atom, the second term of the matrix element in eq. (14) was obtained as a sum of the terms with separated angular and radial parts for electron loss of the projectile electron in the initial bound state with *arbitrary* quantum numbers nl.

One can estimate the order of magnitude of the second (relativistic) term in eq. (14) as

$$\beta\alpha_Z \sim v/c\cdot\langle p_e\rangle/m_e c \sim v/c\cdot v_e/c, \qquad (15)$$

where m_e, v_e and $\langle p_e\rangle$ denote the rest mass, orbital velocity and impulse matrix element for the projectile electron. As seen from eq. (15), the influence of the magnetic interaction is very large if both the ion velocity and the orbital electron velocity are close to the speed of light. This estimation is quite rough because the second term in eq. (14) can be very large even for velocities $v \ll c$ if a transition occurs with a small momentum transfer Q (see [9]).

The formulae obtained in [31] for the electron-loss cross sections in relativistic Born approximation were realized in a computer program called RICODE (Relativistic Ionization CODE) which is described in [7] and appendix. This code is a continuation of the LOSS- and LOSS-R-codes for calculation single-electron loss cross section at high energies including a relativistic energy range.

Calculated relativistic ionization cross sections of H-like uranium ions in the 1s and 2s-states colliding with protons (point-like particle) are shown in Fig. 6. As is seen, RICODE-results are in good agreement with Voitkiv and Najjari calculations [23] if the relativistic interaction and non-relativistic wave functions are used which is the case in the RICODE-program. The use fully relativistic approach, i.e. relativistic interaction and relativistic Dirac wave functions, used in [33] leads to a reduction of the ionization cross section by a factor of 2 compared to RICODE-results. However, as these examples represent the "ultimate" case of strongly bound projectile electrons, the deviation in electron-loss cross sections for many-electron systems is expected to be small because ionization of inner-shell projectile electrons by the target particle gives a very small contribution to the

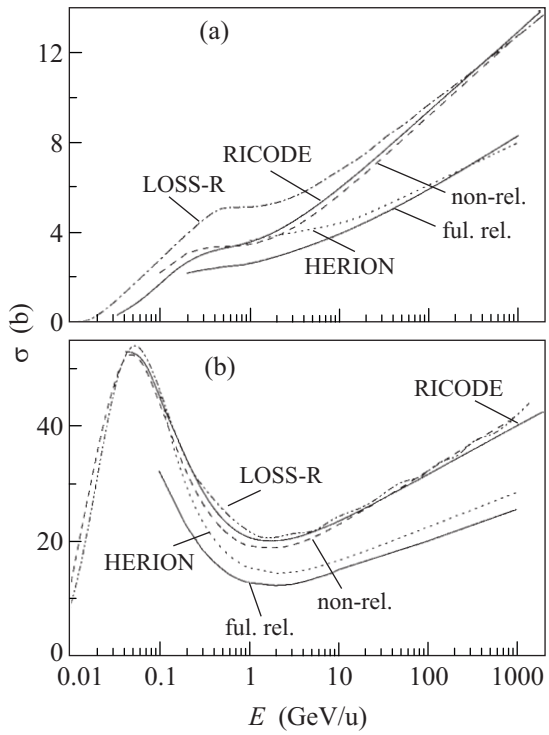

Fig. 6. Calculated cross sections for relativistic ionization of H-like U^{91+} ions in the ground ($1s$) (a) and excited ($2s$) (b) states by proton impact as a function of collision energy. Curves labeled by LOSS-R, RICODE and HERION – calculations by corresponding codes described below; non-rel. – calculated with relativistic interaction and non-relativistic wave functions and ful. rel. – with relativistic interaction and relativistic (Dirac) wave functions [23]

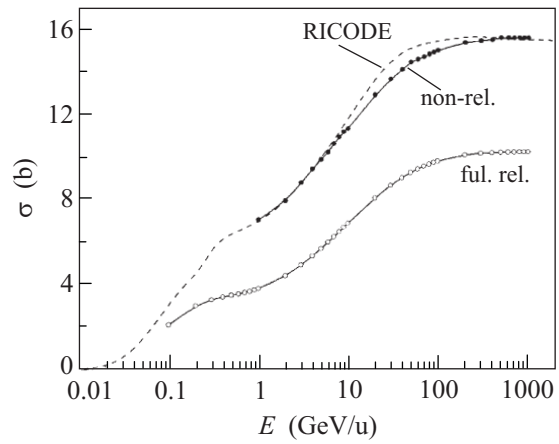

Fig. 7. Calculated cross sections for relativistic ionization of H-like U^{91+} ions in the ground $1s$ state by hydrogen atoms H($1s$) in the ground state as a function of ion energy. Dashed curve – RICODE calculations; non-rel. – calculated with relativistic interaction and non-relativistic wave functions and ful. rel. – with relativistic interaction and relativistic (Dirac) wave functions [23]

total loss cross section. As also seen from the figure, the results by the LOSS-R-code are close to RICODE-calculations and the data by the HERION-code, which uses the relativistic wave functions (section 4), are in quite good agreement with fully relativistic calculations by Voitkiv and Najjari [23]. We note that all calculated cross sections for proton impact increase with energy increasing that is typical for the incident charged particle.

Relativistic electron-loss cross sections of $U^{91+}(1s)$ ions colliding with neutral hydrogen atoms H($1s$) are displayed in Fig. 7. Again, the RICODE-results are in good agreement with Voitkiv and Najjari calculations [23] performed using relativistic interaction and non-relativistic wave functions, and fully relativistic calculations [32] leads to a reduction of the cross section by a factor of 2.

From Figs. 6 and 7 one can see a principally different behavior of relativistic cross sections in collisions with ions (protons, Fig. 6) and neutral atoms (hydrogen, Fig. 7): in the first case, ionization of the projectile electron occurs under interaction with the long-range Coulomb field of the unscreened proton charge and the cross sections increase with energy approximately as $\sigma \sim \ln\gamma$ where γ is the relativistic factor, whereas in collisions with neutrals electron-loss cross sections turn to a constant value at high energies because of the screened target field which is exponentially small at large distances (see [9] and [23] for details).

A typical example of contribution of inner-shell electron removal to the total loss cross sections is shown in Fig. 8 where RICODE-calculations are presented for

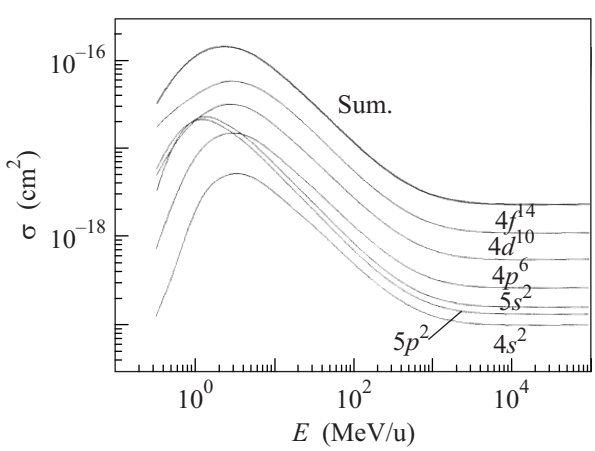

Fig. 8. Contribution of EL cross sections from different shells of U^{28+} ions colliding with Ar atoms to the total EL cross section (sum) as a function of collision energy, RICODE, present work

U^{28+} ions colliding with Ar atoms. As seen, the main contribution is given by electron removal from $4f^{14}$-, $4d^{10}$- and $4p^6$-electronic shells having relatively low binding energies and a large number of equivalent electrons. As expected, at high collision energies all electron-loss cross sections have approximately constant values. A contribution from the electron shells deeper than $4s^2$ can be neglected.

Fig. 9 shows experimental data and theoretical calculations of the total electron loss cross sections for

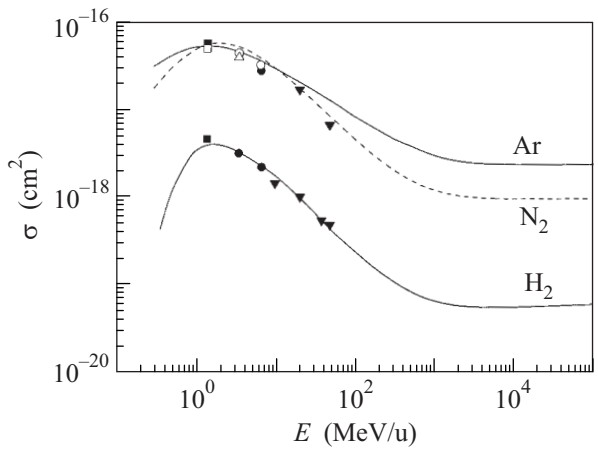

Fig. 9. Total electron loss cross sections in collisions of U^{28+} ions with H_2, N_2 and Ar targets as a function of ion energy. The data for H_2 and N_2 targets are given in units of cm^2/mol. Symbols, experiment – H_2 and N_2 targets: ■ [15], • [16], ▼ [17]; Ar target: □ [5], ∘ [16], △ [6]. Curves – RICODE-calculations [7]

U^{28+} ions colliding with H_2, N_2 and Ar targets over a wide energy range. Theoretical data were obtained using two approaches: a classical approach (DEPOSIT-code) at low and intermediate energies with account for multi-electron loss processes, and quantum-mechanical approach (RICODE-program) which predicts a single-electron loss cross sections at high and relativistic energies (see [7] for details). We note that in [7], a semi-empirical formula for single-electron loss cross sections is suggested based on properties of the relativistic Born approximation and numerical calculations by the RICODE-program.

6. Ion-beam lifetimes. One of the most important application of known electron-loss and capture cross sections is to predict the ion-beam lifetimes τ and beam losses of ions in accelerators and storage rings. The ion-beam lifetime τ is defined by equation:

$$\tau = \left\{ \rho\beta c \sum_T \left[Y_T \sigma_{\rm tot}^{\rm EC}(q, Z_T, v) + Y_T \sigma_{\rm tot}^{\rm EL}(q, Z_T, v) \right] \right\}^{-1}, \quad (16)$$

where v and q denote the ion velocity and ion charge in a beam, respectively, and ρ – the density of residual gas. The sum on T runs over all residual-gas components (H, C, N, O, Ar etc.), where Z_T and Y_T denote their nuclear charges and individual fractions, respectively, so that $\Sigma_T Y_T = 1$. $\sigma_{\rm tot}^{\rm EC}$ and $\sigma_{\rm tot}^{\rm EL}$ are the total electron-capture and loss cross sections, i.e., they account for the multiple-electron capture and loss processes.

As example, the experimental and theoretical data for ion-beam lifetimes of U^{28+} obtained at the SIS-synchrotron at GSI, Darmstadt, are shown in Fig. 10. One can see a good agreement between experimen-

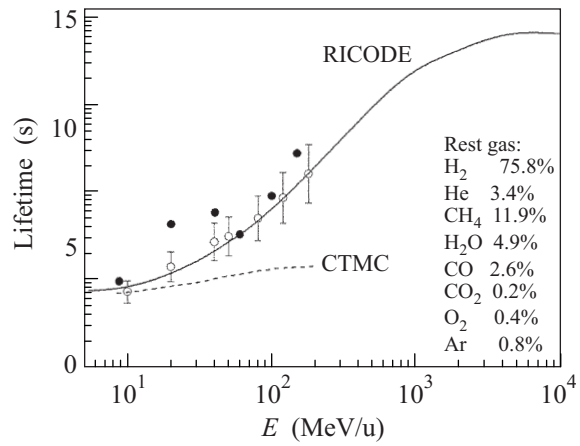

Fig. 10. Ion-beam lifetimes of U^{28+} ions as a function of ion energy at an assumed residual-gas pressure of about 10^{-10} mbar and assumed residual-gas compositions which are indicated in the figure. Experiment: ∘ [17], • [33]. Theory: dashed curve – calculated with CTMC cross sections, solid curve – calculated with RICODE electron-loss cross sections. From [7]

tal measurements and calculations performed by the RICODE-program. We note that in this particular case, the electron-capture cross sections at energies $E > 10$ MeV/u are much smaller than electron-loss cross sections and they are neglected in calculations. At highly relativistic energies, $E > 5$ GeV/u, the predicted lifetime is nearly a constant value which is around 13 s for the assumed vacuum conditions.

Using reliable set of electron-loss and capture cross sections and experimental data for ion-beam lifetimes, one can solve an *inverse* problem using equation (16): to estimate the vacuum conditions (gas pressure and residual-gas components) at which lifetime measurements have been performed. Usually, to determine the vacuum conditions is a very complicated experimental problem.

Conclusion. High-energy electron-loss (projectile ionization) processes of heavy many-electron ions col-

liding with neutral atoms are considered over a wide energy range including relativistic energies. Numerical calculations for electron-loss cross sections of heavy ions colliding with protons and neutral atoms are presented by several computer codes. The best results for many-electron projectiles are obtained by the RICODE computer program based on the relativistic Born approximation. At relativistic energies, in the case of atomic targets electron-loss cross sections exhibit a quasi-constant behavior because of the screened field created by the target atom, and the cross sections increase with energy increasing in the case of ionic targets (protons).

Using accurate data on electron-loss cross sections the experimental ion-beam lifetimes for U^{28+} ions are explained and predicted for ultra-relativistic energies where the lifetime turns to a constant value of about 13 s. Knowing a set of reliable data on electron-loss and capture cross sections and experimental data on the ion-beam lifetimes, it is possible to solve the inverse problem, i.e. to estimate the experimental vacuum conditions such as the residual-gas pressure and its components.

The authors are grateful to A.B. Voitkiv for valuable discussions and to S.N. Andreev for the codes development. This work was performed under the grants # 08-02-00005-a and 11-02-00526-a of the Russian Foundation for Basic Research.

APPENDIX. The RICODE computer program. The RICODE-program (Relativistic Ionization CODE) is intended to calculate single-electron loss cross sections in ion-atom collisions and is based on the relativistic Born approximation. The RICODE is a further development of the LOSS- and LOSS-R-codes described in [14] and [18], respectively.

In the RICODE, the electron-loss cross section for the projectile electronic shell is calculated in the partial-wave representation in the momentum-transfer Q space in the form (cf eqs. (3)–(5)):

$$\sigma_{\rm ion}(v) = \frac{8\pi}{(\beta c)^2}\sum_{nl} N_{nl}\sum_{\lambda}\int\limits_0^\infty d\varepsilon\times$$

$$\int\limits_{Q_0}^\infty \frac{dQ}{Q^3}\left[Z_T^2(Q)F_{nl}^2(Q)+Z_T^2(Q')\frac{\beta^2(1-Q_0^2/Q^2)}{(1-\beta^2Q_0^2/Q^2)^2}G_{nl}^2(Q)\right], \tag{A1}$$

$$Q_0 = \frac{I_{nl}+\varepsilon}{v}, \quad Q' = \sqrt{Q^2-\beta^2Q_0^2}, \tag{A2}$$

where $Z_T(Q)$ denotes the effective charge of the incident particle in the Q-representation, ε and λ – the energy and orbital momentum of the active electron to be ejected, I_{nl} and N_{nl} – the binding energy and number of equivalent electrons of the projectile shell nl, and β is the relativistic factor. The function $F(Q)$ is a usual Born form-factor given by

$$F_{nl}^2(Q) = \sum_{\kappa\lambda}(2\kappa+1)(2\lambda+1)\begin{pmatrix} l & \lambda & \kappa \\ 0 & 0 & 0\end{pmatrix}^2 |R^B(Q)|^2, \tag{A3}$$

$$R^B(Q) = \int\limits_0^\infty P_{nl}(r)P_{\varepsilon\lambda}(r)[j_\kappa(Qr)-\delta_{\kappa 0}]dr,$$
$$|l-\lambda| \le \kappa \le |l+\lambda|, \tag{A4}$$

where the radial wave functions $P(r)$ of the active electron in the bound (nl) and continuum $(\varepsilon\lambda)$ states are calculated numerically by solving the non-relativistic Schrödinger equation in the effective field of the atomic core. The functions $P_{nl}(r)$ and $P_{\varepsilon\lambda}(r)$ are normalized, respectively:

$$\int P_{nl}^2(r)dr = 1, \quad \int P_{\varepsilon\lambda}(r)P_{\varepsilon'\lambda}(r)dr = \pi\delta(\varepsilon-\varepsilon'). \tag{A5}$$

The effective charge of the target particle is calculated in the form:

$$|Z_T(Q)|^2 = \left[Z - \sum_{j=1}^N \langle j|\exp(i\mathbf{Qr})|j\rangle\right]^2 +$$
$$+\left[N - \sum_{j=1}^N |\langle j|\exp(i\mathbf{Qr})|j\rangle|^2\right] \tag{A6}$$

using the Slater nodeless radial functions $|j\rangle$. Here Z and N denote the nuclear charge and number of electrons in the target particle, respectively. For neutral atoms one has $Z = N$.

The second term in (A1) is responsible for the relativistic (magnetic) interaction between colliding particles where the function $G_{nl}(Q)$ depends on the derivative of the radial function $P_{nl}(r)$ and is given by [31]:

$$G_{nl}^2(Q) = \sum_{\kappa\lambda}\frac{2}{137^2}\frac{(2\kappa+1)(2\lambda+1)}{2l+1}\times$$
$$\times\left|i^\kappa\begin{pmatrix}\lambda & \kappa & l+1\\ 0 & 0 & 0\end{pmatrix}[(l+1)R^d(Q)-l(l+1)R^B(Q)]+\right.$$
$$\left.+i^\kappa\begin{pmatrix}\lambda & \kappa & l-1\\ 0 & 0 & 0\end{pmatrix}[lR^d(Q)+l(l-1)R^B(Q)]\right|^2, \tag{A7}$$

$$R^d(Q) = \int\limits_0^\infty P_{\varepsilon\lambda}(r)j_\kappa(Qr)\frac{dP_{nl}(r)}{dr}dr, \tag{A8}$$

where $i^2 = -1$. We note that in relativistic approximation, the effective charge in the second term of eq. (A1) depends on the shifted momentum-transfer Q'.

1. D. Hoffmann, G. Logan, B. Sharkov et al., Phys. Scr. **123**, 1 (2006).
2. G. Kraft, Progr. Part. Nucl. Phys. **45**, 473, 2 (2000).
3. A. V. Melnikov, A. Alonso, E. Ascasibar et al., Fusion Science and Technology **51**, 1 (2007).
4. FAIR Baseline Technical Report, http://www.gsi.de/fair/reports/btr.html.
5. W. Erb, GSI Report P-7-78, October (1978).
6. A. N. Perumal, V. Horvat, R. L. Watson et al., Nucl. Instrum. Meth. B **227**, 251 (2005).
7. V. P. Shevelko, I. L. Beigman, M. S. Litsarev et al., Nucl. Instrum. Methods B **269**, 1455 (2011).
8. J. Eichler and W. E. Meyerhof, *Relativistic Atomic Collisions*, Academic Press, New York, 1995.
9. A. Voitkiv and J. Ullrich, *Collisions of Structured Atomic Particles*, Springer, Berlin, Heidelberg 2008.
10. C. A. Bertulani and G. Baur, Phys. Rep. **163**, 299 (1988).
11. A. B. Voitkiv, Phys. Rep. **392**, 191 (2004).
12. R. E. Olson, Phys. Rev. A **39**, 5572 (1989).
13. V. P. Shevelko, D. Kato, M. S. Litsarev, and H. Tawara, J. Phys. B **43**, 215202 (2010).
14. V. P. Shevelko, Th. Stöhlker, and I. Yu. Tolstikhina, Nucl. Instrum. Methods B **184**, 295 (2001).
15. B. Franzke, IEEE Trans. Nucl. Sci. 28, 2116 (1981).
16. R. E. Olson, R. L. Watson, V. Horvat et al., J. Phys. B **37**, 4539 (2004).
17. G. Weber, C. Omet, R. D. DuBois et al., Phys. Rev. ST Accel. And Beams **12**, 099901 (2009).
18. I. L. Beigman, I. Yu. Tolstikhina, V.P. Shevelko, Technical Physics, 53(5), 547 (2008).
19. H. Bethe, in *Handbuch der Physik*, Springer, Berlin 1933, V. 34, p. 273.
20. V. B. Berestetskii, E. M. Lifshitz, and L. P. Pitaevskii, *Course of Theoretical Physics*, Vol. 4: *Quantum Electrodynamics*, Pergamon, New York, 1982.
21. R. Anholt, W. E. Meyerhof, H. Gould et al., Phys. Rev. A **32**, 3302 (1985).
22. D. M. Davidovic, B. L. Moiseiwitsch, and P. H. Norrington, J. Phys. B **11**, 847 (1978).
23. A. B. Voitkiv, *Electron excitation and loss of highly charged ions in relativistic collisions with atoms*, Doctorate Thesis, P.N. Lebedev Physical Institute, M.: 2010 (in Russian).
24. H. F. Krause, C. R. Vane, S. Datz et al., Phys. Rev. A **63**, 032711 (2001).
25. R. Anholt, and U. Becker, Phys. Rev. A **36**, 4628 (1987).
26. A. H. Sörensen, Phys. Rev. A **58**, 2895 (1998).
27. V. I. Matveev, E. S. Gusarevich, D. U. Matrasulov et al., J. Phys. B **39**, 1447 (2006).
28. B. Najjari, A. Surzhykov, and A. B. Voitkiv, Phys. Rev. A **77**, 042714 (2008).
29. S. N. Andreev, I. L. Beigman, I. Yu. Tolstikhina et al., Bulletin of the Lebedev Physics Institute **35**(3), 89 (2008).
30. A. B. Voitkiv, B. Najjari, and A. Surzhykov, J. Phys. B **41**, 111001 (2008).
31. G. Baur, I. L. Beigman, I. Yu. Tolstikhina et al., Phys. Rev. A **80**, 012713 (2009).
32. http://accelconf.web.cern.ch/accelconf/e02/PAPERS/WEPLE116.pdf.
33. A. Krämer, O. Boine-Frankenheim, E. Mustafin et al., Proc. of EPAC 2002, Paris, 2002.